Wireless Power Transfer for Running EV Powering Using Multi-Parallel Segmented Rails

Kai Song, Chunbo Zhu
School of Electrical Engineering and Automation
Harbin Institute of Technology
Harbin, China
kaisong@hit.edu.cn
zhuchunbo@hit.edu.cn

Kim Ean Koh, Takehiro Imura, Yoichi Hori
The University of Tokyo
Kashiwa, Japan
koh@hori.k.u-tokyo.ac.jp
imura@hori.k.u-tokyo.ac.jp
hori@k.u-tokyo.ac.jp

***Abstract*—The conventional static wireless powering technology for electric vehicles (EV) has the disadvantages of non-running powering and frequent charging times. To solve the above problems, a novel wireless power transfer (WPT) technology for dynamic roadway EV powering using multiple parallel segmented rails is proposed in this paper. Firstly, currently several dynamic powering methods are compared. Then, circuit model and transfer function is established to analyze the topology of this proposed LCL resonator, respectively. Finally, transient response time of the topology is calculated by using the dominant pole method. Both simulation and experimental results demonstrate that the proposed strategy can achieve oven power flow and significant efficiency improvement compared with the traditional structure.**

Keywords—Wireless power transfer; dynamic EV powering; multi-parallel segmentaed rails; transient response time; LCL

I. INTRODUCTION

To save energy and reduce environmental pollution, EVs have been widely accepted in many countries. However, charging has become a bottleneck for the rapid development of EVs. Conventional plug-in charging station is limited to one EV at one time. Furthermore, high voltage is used at the charging station and safety will be another issue. WPT is able to mitigate above mentioned issues. Users only need to drive the car to the designated spot, and the car will begin charging automatically. This technology is known as static wireless powering and is currently available [1]-[4].

However, frequent charging, heavy and costly batteries are still required for static charging. The cruising distance is also insufficient especially for public transportation such as bus. Based on all these reasons, dynamic powering which can supply electrical energy to the moving EVs through wireless power transfer is researched and developed recently [5]-[9]. EVs can therefore carry smaller batteries and even without batteries. Infinity cruising distance can be realized, energy supplying process to EVs is safer and more convenient.

Currently available dynamic powering technology is aiming at solving continuous power transfer issue. The hardware of dynamic powering system mainly consists of underground energy converter & transmitting devices as well as EV's power receiving & converter. The important indexes include energy transfer gap, efficiency, power capability and lateral misalignment distance. Currently, research groups in Korea Advanced Institute of Science and Technology (KAIST), The University of Auckland, Oak Ridge National Laboratory (ORNL) and The University of Tokyo are working on technical issues that are related to dynamic charging, with focus mainly on system modeling, power conversion, magnetic coupling design, magnetic shielding technology, etc. For example, The University of Auckland used long rail to solve the energy transfer path switching issue when the vehicles are moving. A LCL-T circuit was used to automatically adapt to receiver circuits, and transfer efficiency was improved significantly [9]. KAIST utilized the optimized core design in the rails to increase transfer efficiency and distance. The design has been implemented in an actual public transport system [6], [8]. In ORNL, modular coils were arranged along the charging path but transferred power and efficiency were uneven during cruising due to the position of the transmitters and on-board receiver [5].

However, WPT will induce electromagnetic field radiation. At present, electromagnetic shielding such as installing ferrite core or aluminum plate at the bottom of vehicle is commonly used to reduce exposure towards human inside the vehicle. On the other hand, human outside the vehicles, such as pedestrians at the roadside or crossing the road will have high risk of exposure when long rail and high-power dynamic powering application is implemented [10]. Therefore, the improved dynamic powering system is required to solve the electromagnetic interference (EMI) issue.

In this paper, a multi-parallel segmented rails based dynamic roadway wireless powering method is proposed. Using single inverter and multiple modular transmitters, oven magnetic field is formed between the transmitters and receivers and the unstable transfer efficiency issue is solved. Also, transmitters are deactivated through switching when the vehicle moves away, therefore exposure to the surrounding human is avoided.

II. SYSTEM OVERVIEW

A. Scheme Comparison

For running EV powering, the design of underground transmitters is required. According to [2], [3], currently there are two main types of transmitter designs: long rail and

This work is supported by Scientific Research Foundation of the Higher Education Institutions (HIT. NSRIF. 2014018) and Heilongjiang Postdoctoral Sustentation Fund (LBH-Z13077).

978-1-4799-6610-3/15/$31.00 ©2015 IEEE

segmented rail as shown in Fig. 1. This paper is based on magnetically resonant coupling to realize the dynamic powering for EV. Analysis in terms of transmitter and receiver dimension, transfer efficiency, lateral misalignment and EMC are discussed for both long rail and segmented rail solutions.

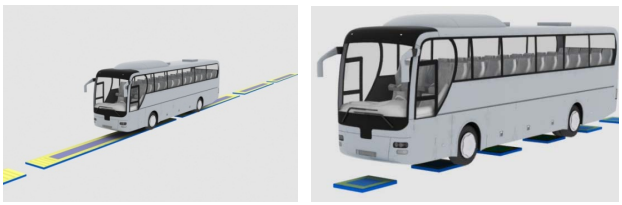

(a) (b)

Fig. 1. Two main dynamic powering methods (a) Long rail; (b) Segment rail.

Firstly, the receiver size is chosen according to the size of the bottom plate of the vehicle (outer size 20×40 cm rectangular coil with 14 turns) and the vertical charging gap is 10 cm. Without loss of generality, the receiver size, height and load in all methods discussed below are the same. Method I, the transmitter and receiver are identical as shown in Fig. 2(a).

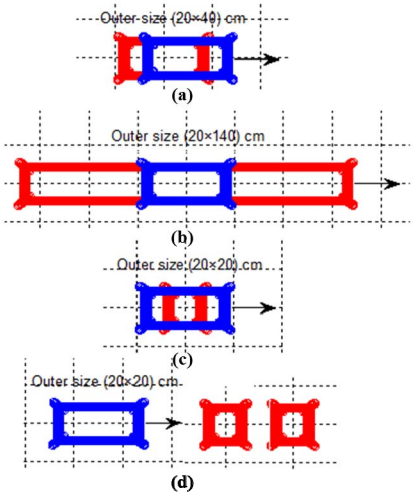

Fig. 2. Comparison of different coupling structures using same receiver and different transmitters. (a) Identical *Tx* and *Rx*) (b) Long *Tx* (c) Half size *Tx* (d) Multi-half size *Tx*.

Fig. 3 shows the maximum transfer efficiency plot *vs*. the receiver lateral displacement. For Method II in Fig. 2(b), the transmitter is with outer size 20×140 cm, 14 turns and is larger than the receiver. The blue line in Fig. 3 shows that the efficiency is maintained at above 90% for large lateral misalignment. In Method III, a single small transmitter (outer size 20×20 cm) is used and the turn number is similarly 14 turns. The green line in Fig. 3 shows that the power transfer is only efficient within a limited lateral displacement. In Method IV, two small transmitters are used consecutively to transfer power to the receiver. All the transmitters are with the same 20×20 cm, the number of turns is 14 and the gaps between two transmitters are 14 cm. From the red line in Fig. 3, the lateral charging coverage is significantly increased compared to single small transmitter and the efficiency is maintained above 85%. In Method V, much longer coil with the dimension 20×1040 cm and 14 turns is employed. From the dotted line in Fig. 3, the efficiency is low (< 80%) due to the higher coil inner resistance of the transmitter. Therefore, consecutive segmented rail method is employed to ensure the stability of power supply and high transfer efficiency.

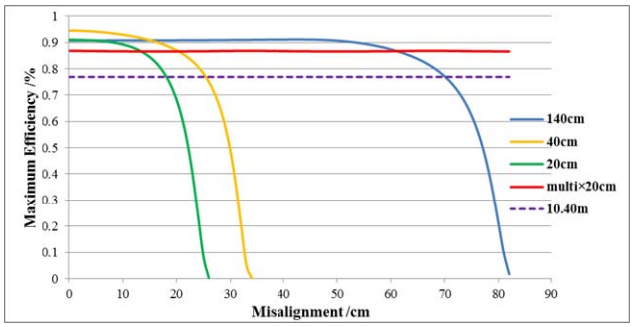

Fig. 3. Maximum efficiency *vs*. lateral misalignment of different transmitter configurations.

The standard outlined by The International Commission on Non-Ionizing Radiation Protection (ICNIRP) is below 200 mA/m^2 at 100 kHz for public exposure. Exposure above this value may cause damage to the functionality of nervous system [11]. The limit for specific absorption rate (SAR) is below 2W/kg and the power density is below 10 W/m^2. Exposure above these limits will cause heating of human cells and tissues as shown in Fig. 4. Given that the disadvantage of high-power long transmitter which has strong radiation exposure when pedestrians wait at the roadside or cross the road, a segment rail based dynamic powering method is proposed in this paper.

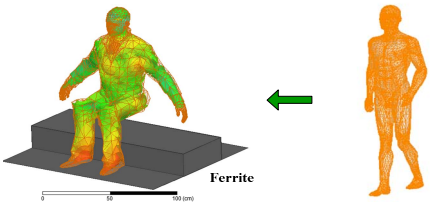

Fig. 4. EMC of dynamic powering system for people inside/outside the EV.

B. *System Design*

Single inverter and multiple parallel segmented rails based dynamic powering strategy is used to ensure stable power and efficiency transfer [12]. Each segmented rail consists of a transmitter, a LCL resonator, a high frequency switching, a magnetic sensor and controller as shown in Fig. 5. Magnetic sensor is employed to detect the position of the vehicle accurately by sensing the changes of the magnetic field strength. Switching control is performed according to the output of the magnetic sensor. Dynamic wireless power transfer can be used to power the AC motor of the running EV directly. When the EV is stopping, for example, at the traffic lights, the dynamic WPT system is used to charge the on-board battery. Therefore the cruising distance can be extended.

978-1-4799-6610-3/15/$31.00 ©2015 IEEE

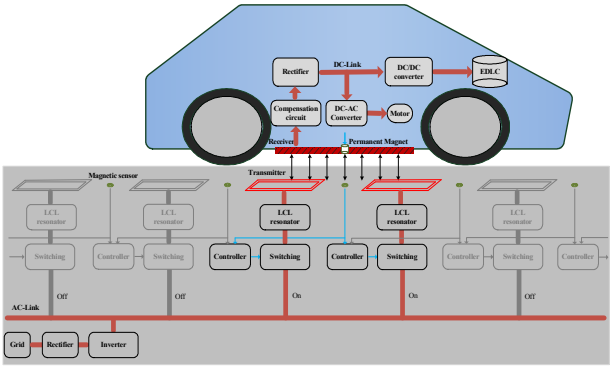

Fig. 5. Diagram of multi-parallel segmented rails based dynamic powering system.

III. Analytical Models

A. Circuit Topology

The major demerit of basic *SS* compensation structure is that the input impedance of the inverter is related to the AC equivalent load R_L. Furthermore, the voltage source v_1 is short-circuited in the case of no load so that a large primary side current i_{11} is introduced. To solve the problem, a LCL resonator composed of a track inductor L_{11} and a parallel capacitor C_{11} is employed in the traditional primary side serial topology (serial capacitor C_{12} and transmitter L_{12}). The LCL resonator is used to increase the passive power compensation for adapting the load changes. Thus, it improves the stability and reliability of the system.

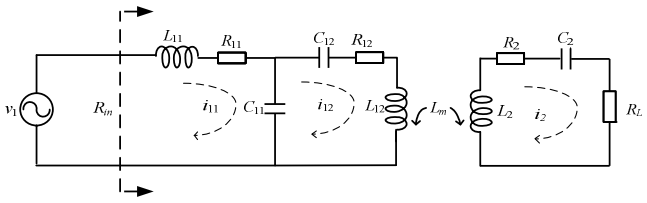

Fig. 6. Equivalent circuit of primary side LCL resonator.

where L_m is the mutual inductance, i_{11} is the primary side current, i_{12} is the transmitter current, i_2 is the secondary side current, R_{11} is the inner resistance of L_{11}, R_{12} is the inner resistance of L_{12}, R_2 is the inner resistance of receiver L_2, and R_{in} is the primary side equivalent impedance and described as:

$$R_{in} = R_{11} + \frac{\omega^2 L_{11}^2}{(R_{12} + \frac{\omega^2 L_m^2}{R_2 + R_L})} \approx \frac{\omega^2 L_{11}^2}{R_{12} + \frac{\omega^2 L_m^2}{R_2 + R_L}} \quad (1)$$

Obviously, when the EV (receiver) yet enters the rail, it means that the secondary side is equivalent to open-circuit, i.e. $R_L = \infty$. Since $R_{12} \approx 0$, then $R_{in} = \infty$. It indicates that the primary side current i_{11} is small and the inverter output power is just coil loss. When the EV is entering the rail, both R_L and L_m are changing, but R_{in} is relatively small and i_{11} increases. Then, the inverter can output a high power. Thus, the LCL resonator plays a role of automatic impedance matching which is not only able to control the primary side output power automatically, but also has a high transfer efficiency during loaded and low loss during unloaded (only coil loss).

TABLE I. Parameters of Designed LCL Resonators

Symbol	Meaning	Value
L_{11}	Primary side track inductor	30 μH
R_{11}	Primary side track resistance	0.1 Ω
C_{11}	Primary side parallel capacitor	117 nF
L_{12}	Primary side transmitter inductance	49 μF
R_{12}	Primary side transmitter resistance	0.2 Ω
C_{12}	Primary side compensation capacitor	184.5 nF
L_2	Secondary side receiver inductance	93 μH
R_2	Secondary side receiver resistance	0.33 Ω
C_2	Secondary side compensation capacitor	37.7 nF
R_L	AC equivalent load resistance	10 Ω
l_Tx	Transmitter length	20 cm
l_Rx	Receiver length	40 cm
ω_0	Resonant frequency	85 kHz
L_m	Mutual inductance of double resonators	8.3μH

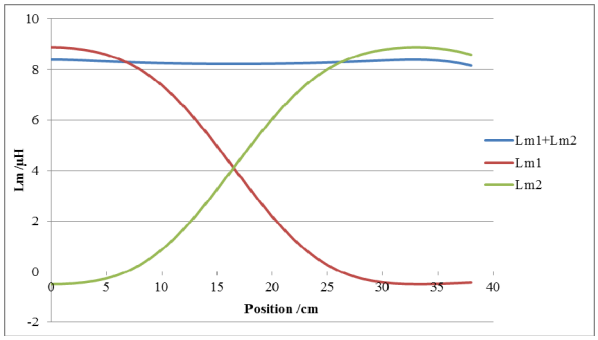

Fig. 7. Mutual inductance of two parallel LCL resonators.

To ensure the stability of power & efficiency, a double LCL parallel small transmitters and big receiver is designed using the above Method IV. All the capacitors and inductors are identical in each sub-LCL resonator as shown in Table I. Here, mutual inductance is calculated by Neumann formula [13] and mutual inductance between two transmitters is 0. When the circuit works at the resonant frequency ω_0, the parameters are defined as:

$$\begin{cases} \omega_0 L_{11} = \dfrac{1}{\omega_0 C_{11}} = \omega_0 L_{12} - \dfrac{1}{\omega_0 C_{12}} \\ \omega_0 L_2 = \dfrac{1}{\omega_0 C_2} \end{cases} \quad (2)$$

Fig. 7 shows the total mutual inductance L_m of the two parallel LCL resonators as well as single mutual inductance L_{m1} and L_{m2} of each sub-resonator, respectively. Obviously, the total mutual inductance of the designed double parallel LCL transmitters is equivalent with the sum of the two independent sub-resonators, i.e. $L_m = L_{m1} + L_{m2}$. According to the equivalent circuit equation of double LCL parallel resonators, the transmitter current is derived as:

$$i_{12f} = i_{12s} = i_{12} \approx -j\omega_0 C_{11} v_1 \quad (3)$$

The secondary side current is written as:

$$i_2 = \frac{j\omega_0 (L_{m1} + L_{m2})}{R_2 + R_{ac}} i_{12} = \frac{\omega_0^2 C_{11} (L_{m1} + L_{m2})}{R_2 + R_{ac}} v_1 \quad (4)$$

978-1-4799-6610-3/15/$31.00 ©2015 IEEE

The load output power is descried as:

$$P_L = |i_2|^2 R_L = \frac{(\omega_0^2 C_{11})^2 (L_{m1} + L_{m2})^2 R_L}{(R_2 + R_L)^2} V_1^2 \quad (5)$$

Furthermore, the primary side currents of each sub-resonator are given as:

$$\begin{cases} i_{11f} = \dfrac{R_{12}R_2 + R_{12}R_L + \omega_0^2 L_{m1}(L_{m1} + L_{m2})}{R_2 + R_L} \omega_0^2 C_{11}^2 v_1 \\ i_{11s} = \dfrac{R_{12}R_2 + R_{12}R_L + \omega_0^2 L_{m2}(L_{m1} + L_{m2})}{R_2 + R_L} \omega_0^2 C_{11}^2 v_1 \end{cases} \quad (6)$$

The total current of primary side is given as:

$$i_1 = \frac{2(R_{12}R_2 + R_{12}R_L) + \omega_0^2 (L_{m1} + L_{m2})^2}{R_2 + R_L} \omega_0^2 C_{11}^2 v_1 \quad (7)$$

The primary side input power and transfer efficiency is described as:

$$P_{in} = |i_1|^2 R_{in} = \frac{2(R_{12}R_2 + R_{12}R_L) + \omega_0^2 (L_{m1} + L_{m2})^2}{R_2 + R_L} \omega_0^2 C_{11}^2 V_1^2 \quad (8)$$

$$\eta = \frac{P_L}{P_{in}} = \frac{R_L (\omega_0 L_{m1} + \omega_0 L_{m2})^2}{(R_2 + R_L)(2R_{12}R_2 + 2R_{12}R_L + (\omega_0 (L_{m1} + L_{m2}))^2)} \quad (9)$$

Based on (5) and (9), the output power and transfer efficiency are only related with the AC equivalent load R_L if L_{m1} + L_{m2} is constant. Thus, the stable transfer power & efficiency is guaranteed.

B. Conductance Network Model

According to the equivalent circuit model of the WPT system, the transfer functions of primary side voltages to secondary side currents are derived as:

$$G_{21}(s) = \frac{I_2(s)}{V_1(s)} = \frac{b_3 s^3}{s^6 + a_5 s^5 + a_4 s^4 + a_3 s^3 + a_2 s^2 + a_1 s + a_0} \quad (10)$$

where the polynomial coefficients are given by

$$b_3 = \frac{L_m}{C_{11}L_{11}(L_{12}L_2 - L_m^2)}$$

$$a_5 = \frac{L_{11}L_{12}(R_2 + R_{ac}) + L_{11}L_2R_{12} + (L_{12}L_2 - L_m^2)R_{11}}{L_{11}(L_{12}L_2 - L_m^2)}$$

$$a_4 = \frac{C_2L_2(C_{12}L_{12} + R_{11}R_{12}C_{11}C_{12} + C_{11}L_{11} + C_{12}L_{11}) + C_{11}C_{12}C_2(L_{11}R_{12} + L_{12}R_{11})(R_2 + R_{ac}) + C_{11}C_{12}L_{11}L_{12} - C_{12}C_2L_m^2}{C_{11}C_{12}C_2L_{11}(L_{12}L_2 - L_m^2)}$$

$$a_3 = \frac{C_2(R_2 + R_{ac})(C_{12}L_{12} + R_{11}R_{12}C_{11}C_{12} + C_{11}L_{11} + C_{12}L_{11}) + C_2L_2(R_{12}C_{12} + R_{11}C_{11} + R_{11}C_{12}) + C_{11}C_{12}(L_{11}R_{12} + L_{12}R_{11})}{C_{11}C_{12}C_2L_{11}(L_{12}L_2 - L_m^2)}$$

$$a_2 = \frac{C_2(R_2 + R_{ac})(R_{12}C_{12} + R_{11}C_{11} + R_{11}C_{12}) + (C_{12}L_{12} + R_{11}R_{12}C_{11}C_{12} + C_{11}L_{11} + C_{12}L_{11}) + C_2L_2}{C_{11}C_{12}C_2L_{11}(L_{12}L_2 - L_m^2)}$$

$$a_1 = \frac{R_{12}C_{12} + R_{11}C_{11} + R_{11}C_{12} + C_2(R_2 + R_{ac})}{C_{11}C_{12}C_2L_{11}(L_{12}L_2 - L_m^2)}$$

$$a_0 = \frac{1}{C_{11}C_{12}C_2L_{11}(L_{12}L_2 - L_m^2)}$$

Similarly, the primary side equivalent conductance is available as:

$$G_1(s) = \frac{I_1(s)}{V_1(s)} = \frac{1}{R_{in}(s)} \quad (11)$$

Obviously, the WPT system is a linear sixth-order system. In mathematics, this means (10) has multi-pole that may affect stability and response time of the system. Fig. 8 shows the bode plot of the WPT forward channel. Fig. 9 shows the time-domain waveform and frequency-domain spectrum of the secondary side current. It can be seen that the WPT topology acts as a bandpass filter. Only the fundamental harmonic of the inverter rectangular voltage is passed and all the higher order harmonics are filtered. Thus, the secondary side current waveform is always sinusoidal and the conduction angle is 0° at the operating frequency (85 kHz). Since the value of R_{11} is very small, this does not add additional losses and change the efficiency.

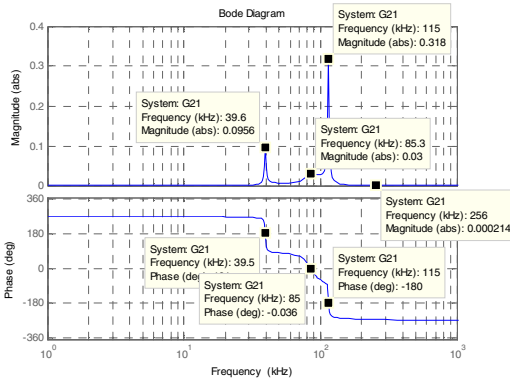

Fig. 8. Bode plot of the WPT forward channel.

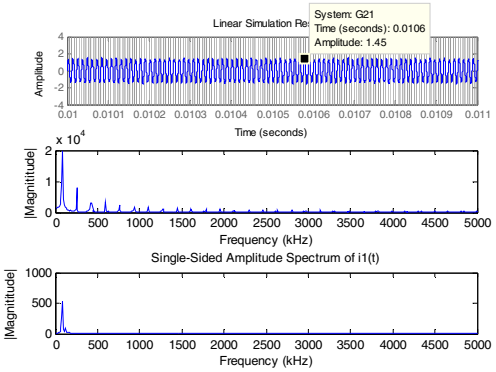

Fig. 9. Waveform and spectrum of secondary side current.

Also, Fig. 10 shows the bode plot of the primary side equivalent conductance $G_1(s)$. It can be seen that the magnitude of third harmonic (256 kHz) of the primary current is larger than the fundamental harmonic (84.9 kHz), which will cause a high current harmonic distortion.

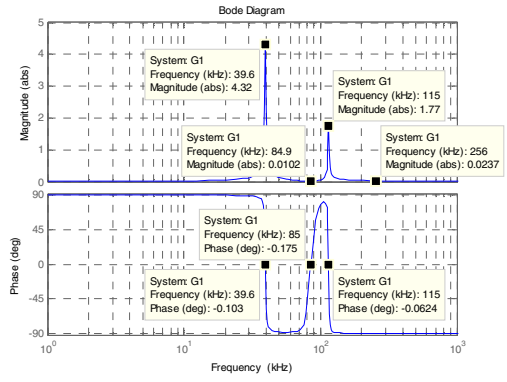

Fig. 10. Bode plot of the primary side equivalent conductance.

C. Transient Response Time

It is important to calculate the transient response time of the designed WPT system when the EV is displaced from the track. This decides the effective powering range after the EV re-entering the track. If the transient response time is enough short, it indicates that the WPT system is able to response quickly. The higher-order step response of the system can be written as:

$$C(s)=\frac{b_0 s^m+b_1 s^{m-1}+\cdots+b_{m-1}s+b_m}{a_0 s^n+a_1 s^{n-1}+\cdots+a_{n-1}s+a_n}=\frac{K_r\prod_{i=1}^{m}(s-z_i)}{\prod_{j=1}^{q}(s-p_j)\prod_{k=1}^{r}(s^2+2\zeta_k\omega_k s+\omega_k^2)}\frac{1}{s} \quad (12)$$

$$=\frac{A_0}{s}+\sum_{j=1}^{q}\frac{A_j}{s-p_j}+\sum_{k=1}^{r}\frac{B_k s+C_k}{s^2+2\zeta_k\omega_k s+\omega_k^2}$$

$$c(t)=L^{-1}[C(s)]=A_0+\sum_{j=1}^{q}A_j e^{p_j t}+\sum_{k=1}^{r}A_k e^{-\zeta_k\omega_k t}\sin\left[\omega_{dk}t+\varphi_k\right] \quad (13)$$

Based on the dominant pole method, the step response curve is related to closed loop poles and zeros， and the high order response characteristic is mainly from poles that are near to imaginary axis and far from zero. The sixth-order dominant poles are two complex conjugate poles. Thus, the WPT response can be approximated by the response of second-order system. Then, the setting time *Ts* is derived as 0.8 ms (in Fig. 11).

For dynamic segmented rails powering, the powering time *Tp* can be calculated through the non-zero mutual inductance *vs.* lateral displacement. For example, when the EV velocity is 72 km/h (i.e. 2 cm/ms), and *Tp* can be computed as 10 ms through Fig. 7. Since *Ts* << *Tp*, this system can achieve a rapid response for the running EV.

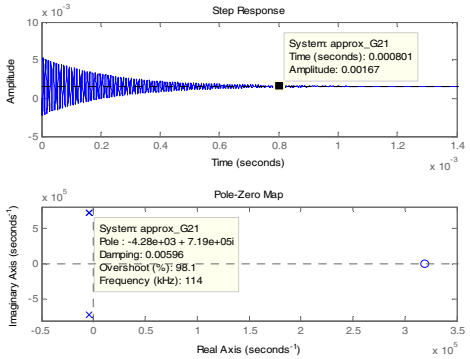

Fig. 11. Time response and pole-zero map of approximated 2nd-order system.

IV. Experiment Validation

To validate the proposed method, an experimental setup was constructed in the laboratory with two small LCL transmitters and a big receiver (Fig. 12). The coil parameters in experiment are identical with that in Table I. Fig. 13 (a) shows the waveforms of v_1, i_{12} and i_2 when R_L = 5 Ω. The secondary side current and transfer efficiency measured by power meter at different lateral displacements (from 0 cm to 34 cm) are shown in Table II. Experimental results demonstrate that the system has stable power flow and transfer efficiency when the receiver is moving.

TABLE II. Results of Dynamic Powering for Moving Load

Lateral Displacement (cm)	RMS of Receiver Current (A)	Efficiency (%)
0	1.31	83.35
3	1.29	81.89
6	1.28	81.61
9	1.28	81.65
12	1.28	81.63
15	1.29	81.35
18	1.31	81.50
21	1.37	83.03
24	1.40	83.12
27	1.41	83.09
30	1.38	82.76
33	1.37	82.26

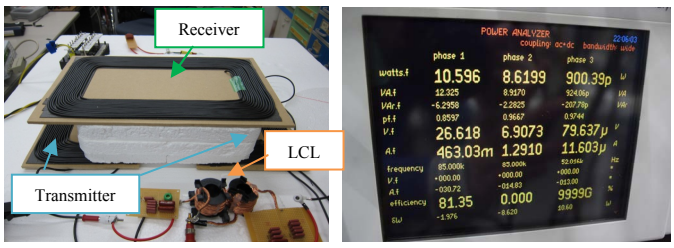

(a) (b)

Fig. 12. Experimental setup a) transmitter and receiver b) measurement results using power meter.

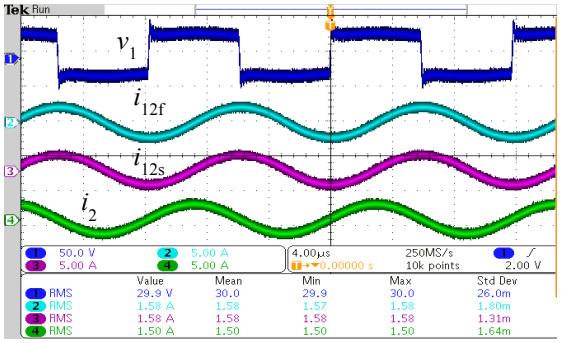

(a)

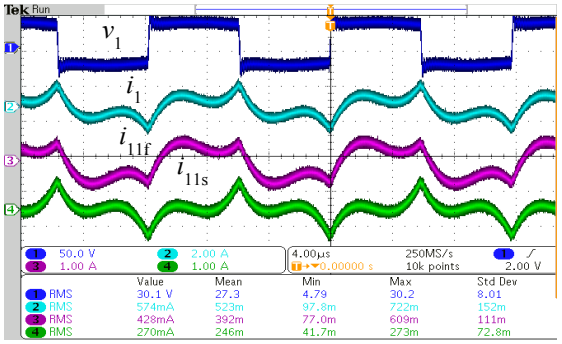

(b)

Fig. 13. Experimental operating waveforms (a) Experimental operating waveforms of primary side voltage v_1, two transmitter current i_{12} and receiver current i_2 when R_L=10Ω; (b) Primary side currents at 0 cm lateral displacement.

Also, the primary side current waveform at 0 cm lateral displacement is shown in Fig. 13 (b). It is obvious that the harmonic distortion exists in the each sub-parallel primary

978-1-4799-6610-3/15/$31.00 ©2015 IEEE

side current. That's because the LCL resonator acts as a bandpass filter, passing both the fundamental and higher order harmonic of the square wave of the voltage source. Theoretical analysis in Fig. 10 is consistent with the experimental results.

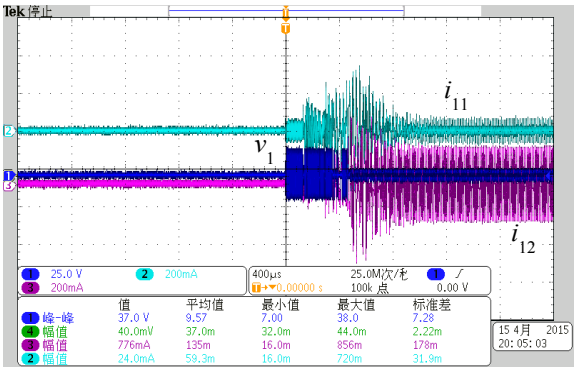

Fig. 14. Experimental step response of primary side voltage v_1, transmitter current i_{12} and primary side current i_{11} at no-load condition.

In order to verify the transient response time of the LCL resonator, the step response is generated by turning on the switching in the AC link. As can be seen in Fig. 14, significant transient overshoots exist in v_1, i_{11} and i_{12} at no-load condition (i.e. EV is not entering the track) due to the underdamped resonator. The setting time measured by the oscilloscope is approximately 800 µs which has a good match with the theoretical step response in Fig. 11.

V. Conclusion

To ensure the stable and oven power transfer, this paper proposed the multi-parallel segmented rails strategy for running EV powering. Comparison in terms of transmitter and receiver dimension, transfer efficiency, lateral displacement and EMC were given for both long and segmented rail solutions. Also, the time/frequency characteristic of LCL resonator was obtained. The transient response and harmonic distortion was analyzed. Experimental results demonstrate the possibility of this method for future roadway powering application.

References

[1] S. Li, and C. Mi, "Wireless power transfer for electric vehicle applications," *IEEE J. Emerging Sel. Topics Power Electron.*, vol. 3, no. 1, pp. 4–17, Mar. 2015.

[2] G. A. Covic and J. T. Boys, "Modern trends in inductive power transfer for transportation applications," *IEEE J. Emerging Sel. Topics Power Electron.*, vol. 1, no. 1, pp. 28–41, Mar. 2013.

[3] G. Nagendra, G. Covic, and J. Boys, "Determining the physical size of inductive couplers for IPT EV systems", *IEEE J. Emerging Sel. Topics Power Electron.,* vol. 2, no. 3, pp. 571–583, Sep. 2014.

[4] W. X. Zhong, X. Liu, and S. Y. Hui, "A novel single-layer winding array and receiver coil structure for contactless battery charging systems with free-positioning and localized charging features," *IEEE Trans. Ind. Electron.*, vol. 58, no. 9, pp. 4136–4144, Sep. 2011.

[5] J. M. Miller, O. Onar, C. White, S. Campbell, C. Coomer, L. Seiber, R. Sepe, and A. Steyerl, "Demonstrating dynamic wireless charging of an electric vehicle: The benefit of electrochemical capacitor smoothing," *IEEE Trans. Power Electron. Mag.*, vol. 1, no.1, pp. 12–24, 2014.

[6] J. Shin, S. Shin, Y. Kim, S. Ahn, S. Lee, G. Jung, S.-J. Jeon, and D.-H. Cho, "Design and implementation of shaped magnetic-resonance-based wireless power transfer system for roadway-powered moving electric vehicles," *IEEE Trans. Ind. Electron.*, vol. 61, no. 3, pp. 1179–1192, Mar. 2014.

[7] W. Y. Lee, J. Huh, S. Y. Choi, X. V. Thai, J. H. Kim, E. A. Al-Ammar, M. A. El-Kady, and C. T. Rim, "Finite-width magnetic mirror models of mono and dual coils for wireless electric vehicles," *IEEE Trans. Power Electron.*, vol. 28, no. 3, pp. 1413–1428, Mar. 2013.

[8] J. Huh, S. W. Lee, W. Y. Lee, G. H. Cho, and C. T. Rim, "Narrow-width inductive power transfer system for online electrical vehicles," *IEEE Trans. Power Electron.*, vol. 26, no. 12, pp. 3666–3679, Dec. 2011.

[9] H. Hao, G. A. Covic, and J. T. Boys, "An approximate dynamic model of LCL-T based Inductive Power Transfer power supplies," *IEEE Trans. Power Electron*., vol. 29, no. 10, pp. 5554-5567, Oct. 2014.

[10] H. H. Wu, A. Gilchrist, K. D. Sealy, and D. Bronson, "A high efficiency 5 kW inductive charger for EVs using dual side control," *IEEE Trans. Ind. Inform.*, vol. 8, no. 3, pp. 585–595, Aug., 2012.

[11] F. Wen, X. Huang, J. Guo, H. Qiang, Y. Xu and Y. Wang, "Study on Efficiency of Electric Vehicles mobile Charging," *International Conference on Wireless Power Transmission Technology and Application (ICWPT2014)*, Nanjing, China, November 14-16, 2014.

[12] K. Song, C. Zhu, Y. Guo, Y. Li, J. Jiang and J. Zhang, "Wireless power transfer for running electric vehicle charging using multi-parallel primary coils," *International Conference on Wireless Power Transmission Technology and Application (ICWPT2014)*, Nanjing, China, November 14-16, 2014.

[13] T. Imura and Y. Hori, "Maximizing air gap and efficiency of magnetic resonant coupling for wireless power transfer using equivalent circuit and Neumann formula," *IEEE Trans. Ind. Electron.*, vol. 58, no. 10, pp. 4746–4752, Oct. 2011.

978-1-4799-6610-3/15/$31.00 ©2015 IEEE